Identification of the orbital pairing symmetry in UPt_3

Matthias J. Graf,[1] S.-K. Yip,[2,3] and J. A. Sauls[2]
[1]*Theoretical Division, Los Alamos National Laboratory, Los Alamos, New Mexico 87545*
[2]*Department of Physics & Astronomy, Northwestern University, Evanston, Illinois 60208*
[3]*Physics Division, National Center for Theoretical Sciences, Hsinchu 300, Taiwan*
(Received 5 January 2000; revised manuscript received 12 June 2000)

This paper summarizes the results of a comprehensive analysis of the thermodynamic and transport data for the superconducting phases of UPt_3. Calculations of the transverse sound attenuation as a function of temperature, frequency, polarization, and disorder are presented for the leading models of the superconducting order parameter. Measurements of the specific heat, thermal conductivity, and transverse sound attenuation place strong constraints on the orbital symmetry of the superconducting order parameter. We show that the superconducting *A* and *B* phases are in excellent agreement with pairing states belonging to the odd-parity E_{2u} orbital representation.

I. INTRODUCTION

Unconventional superconductivity, the electronic analog of superfluidity in ^{3}He, was discovered in the heavy-fermion metals UBe_{13} and UPt_3 more than a decade ago.[1,2] As in liquid ^{3}He the observation of multiple superconducting phases was the direct evidence for a multi-component superconducting order parameter.[3–6] The phases of UPt_3 have since become a paradigm for unconventional superconductivity. However, unlike the case of ^{3}He the identification of the orbital and spin symmetry of the order parameter has been a more difficult task. Heavy fermion metals are more complex materials in which disorder, magnetism, spin-orbit coupling and anisotropy must be factored into any realistic theory of superconductivity in these systems (cf. Refs. 7 and 8).

In this paper we present new theoretical results and analysis of the transport properties of the leading models for the superconducting phases of UPt_3. These models yield qualitatively different predictions for the transport properties in the superconducting phases. We calculate the ultrasonic attenuation for the *A* and *B* phases and discuss its sensitivity to order parameter symmetry, polarization direction and disorder. From our analysis of experimental data for the heat capacity,[9] thermal conductivity,[10,11] and transverse sound attenuation[12] we determine the topology of the excitation gap on the Fermi surface and conclude that the orbital symmetry of the order parameter in the *A* and *B* phases of UPt_3 belongs to an odd-parity E_{2u} representation.

II. PAIRING SYMMETRY

The discoveries of multiple superconducting phases[3–5,13,14] of UPt_3 led to several theoretical models for the superconducting phase diagram based on different symmetry groups, or symmetry breaking scenarios.[15–21] One class of models is based on a two-dimensional (''*E*'') representation of the hexagonal point group, D_{6h}, with the multicomponent superconducting order parameter coupled to a *symmetry breaking field* (SBF). There are four *E*-representations for strong spin-orbit coupling: two *E*-reps for both even-parity (E_{1g},E_{2g}) and odd-parity (E_{1u},E_{2u}) pairing. The *E*-rep models require a weak SBF that lowers the symmetry of the normal state, splits the superconducting transition, and produces multiple superconducting phases.[15] The SBF is generally assumed to be the in-plane antiferromagnetic order parameter that onsets at $T_N \simeq 5$ K;[22] however, other explanations of the SBF have been suggested.[23–25] The precise structure of the short-range AFM correlations, e.g., the spatial structure of domains, as well as the role of AFM as a SBF for superconductivity, is still an open question.[26] One of the outcomes of the calculations summarized below is that a simple model of equal-size, equally populated multidomain structures for the SBF is in disagreement with the anisotropy of the sound attenuation.

The models that have been most successful in explaining the properties of the superconducting phases of UPt_3 are based on the even-parity (E_{1g}) and the odd-parity (E_{2u}) representations of the hexagonal point group. The E_{1g} representation is a realization of spin-singlet, *d*-wave pairing for a metal with a uniaxial symmetry, while the E_{2u} model describes the hexagonal analog of spin-triplet, *f*-wave pairing. These pairing states have an orbital order parameter of the form $\Delta(\mathbf{p}_f) = \eta_1 \mathcal{Y}_1(\mathbf{p}_f) + \eta_2 \mathcal{Y}_2(\mathbf{p}_f)$, where $\mathcal{Y}_{1,2}(\mathbf{p}_f)$ are the basis functions for the appropriate *E*-representation, and the amplitudes $\boldsymbol{\eta} = (\eta_1, \eta_2)$ transform as a two-component ''vector'' under the same *E*-representation. Thus, in the *E*-representations the order parameter of the *A* phase is identified as $\boldsymbol{\eta} = (1,0)$, the *B* phase as $\boldsymbol{\eta} = (1,i)$, and the *C* phase as $\boldsymbol{\eta} = (0,1)$ (see Fig. 1). These identifications then refer to the specific basis functions, $\mathcal{Y}_{1,2}(\mathbf{p}_f)$, for a particular *E*-representation given in Table I. The orbital order parameter differs significantly for the two models, particularly for the high temperature *A* phase ($\eta_2 = 0$). For E_{1g} pairing the *A* phase has the structure, $\Delta_A \sim p_z p_x$, which has an equatorial line node in the basal plane, as well as a longitudinal line node circumscribing the Fermi surface. For the E_{2u} representation, $\Delta_A \sim p_z (p_x^2 - p_y^2)$ also has an equatorial line node, but has *two* longitudinal line nodes oriented 90 degrees to one another. The low-temperature *B* phase of both models breaks time-reversal symmetry (with $\eta_2 \simeq \pm i \eta_1$). As a result the

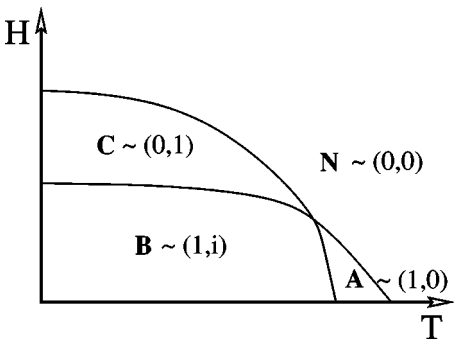

FIG. 1. The phase diagram of UPt_3. The three superconducting phases *A*, *B*, and *C* with amplitudes $\boldsymbol{\eta}=(\eta_1,\eta_2)$ meet with the normal state (*N*) at the tetracritical point. For simplicity the additional two Meissner phases are not shown.

longitudinal line nodes are closed by the growth of the second component of the order parameter; and for $T\to 0$, $\Delta_B \sim p_z(p_x+ip_y)$ for E_{1g} symmetry, while $\Delta_B \sim p_z(p_x+ip_y)^2$ for the E_{2u} representation. Thus, the low energy excitation spectra for the *B* phase of the E_{1g} and E_{2u} models is described by an equatorial line of zero energy excitations ($p_z=0$) and pairs of point nodes of the excitation gap ($p_x=p_y=0$) on the Fermi surface. There is a slight difference in the density of states from the point nodes because the gap varies linearly near the point nodes for the E_{1g} model, $|\Delta(\mathbf{p}_f)| \sim |\vartheta|$, but quadratically for the E_{2u} model, $|\Delta(\mathbf{p}_f)| \sim |\vartheta|^2$. These slight differences are predicted to be observable in the heat transport at ultralow temperatures.[27–29]

All of the *E*-rep models are based on two-component orbital order parameters. However, they yield different predictions for the thermodynamic, magnetic and transport properties, including the *H-T* phase diagram. One important difference arises for the case of weak in-plane hexagonal anisotropy, as is reflected by the very small in-plane anisotropy of H_{c2}.[30,31] Weak in-plane anisotropy leads to an apparent tetracritical point for all field orientations provided the order parameter belongs to an E_2 orbital representation.[7]

A key difference between the even-parity and odd-parity *E*-representations is the spin structure of the order parameter. Odd-parity representations are spin-triplet pairing states, and in the absence of spin-orbit coupling the dimensionality of these representations is three times larger than that of the corresponding spin-singlet *E*-representations. However, strong spin-orbit coupling in the uranium-based heavy fermion metals reduces the symmetry group by allowing only joint rotations of the spin and orbital degrees of freedom. The even and odd parity representations are still described by (pseudo) spin-singlet and spin-triplet order parameters of the form[32–34]

$$\Delta_{\alpha\beta}(\mathbf{p}_f)=\Delta(\mathbf{p}_f)\,(i\sigma_y)_{\alpha\beta} \quad \text{(singlet)}, \tag{1}$$

$$\Delta_{\alpha\beta}(\mathbf{p}_f)=\mathbf{\Delta}(\mathbf{p}_f)\cdot(i\boldsymbol{\sigma}\sigma_y)_{\alpha\beta} \quad \text{(triplet)}. \tag{2}$$

The triplet representations transform only under *joint* spin and orbital rotations of the discrete point group for the normal state, i.e., $\mathbf{\Delta}(\mathbf{p}_f)\to\mathcal{R}\mathbf{\Delta}(\mathcal{R}^{-1}\mathbf{p}_f)$, where the rotation $\mathcal{R}\in[D_{6h}]_{\text{spin-orbit}}$. The full symmetry group of the normal state is $\mathcal{G}=[D_{6h}]_{\text{spin-orbit}}\times\mathcal{T}\times U(1)$ with $[D_{6h}]_{\text{spin-orbit}}$ representing the hexagonal point group with inversion, $\mathcal{T}$ is the time-inversion operation and $U(1)$ is the group of gauge transformations. In the limit of no spin-orbit coupling $\mathbf{\Delta}(\mathbf{p}_f)$ transforms as a spin vector under the vector representation of the full spin-rotation group, and separately as a representation of the point group with respect to the orbital momentum, $\mathbf{p}_f$, i.e., $\mathbf{\Delta}(\mathbf{p}_f)\to\mathcal{R}_{\text{spin}}\mathbf{\Delta}(\mathcal{R}^{-1}_{\text{orbit}}\mathbf{p}_f)$, where $\mathcal{R}_{\text{spin}}\in SU(2)_{\text{spin}}$ and $\mathcal{R}_{\text{orbit}}\in[D_{6h}]_{\text{orbit}}$. In the absence of spin-orbit coupling the enlarged symmetry group for the normal state is $\mathcal{G}=SU(2)_{\text{spin}}\times[D_{6h}]_{\text{orbit}}\times\mathcal{T}\times U(1)$.

There are two special classes of spin-triplet order parameters that are frequently discussed as candidates for the phases of UPt_3. The first class are states in which the spin-triplet order parameter factorizes into a single spin-vector and an orbital amplitude, i.e., $\mathbf{\Delta}(\mathbf{p}_f)=\mathbf{d}\,\Delta(\mathbf{p}_f)$ where $\mathbf{d}$ is a real unit vector and $\Delta(\mathbf{p}_f)$ is an odd-parity orbital function. The vector $\mathbf{d}$ defines the axis along which the pairs have zero spin projection, e.g., if $\mathbf{d}\|\mathbf{z}$, then $\Delta_{\uparrow\uparrow}=\Delta_{\downarrow\downarrow}=0$ and $\Delta_{\uparrow\downarrow}=\Delta_{\downarrow\uparrow}=\Delta(\mathbf{p})$. Here $\mathbf{z}$ is a unit vector in spin space. If we choose the quantization axis to be perpendicular to $\mathbf{d}$, i.e., $\mathbf{d}\perp\mathbf{z}$, then the same pairing state is described as *equal spin*

TABLE I. Polynomial functions representing the symmetry of the low-temperature *B* phases of several pairing models. The first three entries are based on the symmetry group $[D_{6h}]_{\text{spin-orbit}}\times\mathcal{T}\times U(1)$. The third entry is representative of the class of *AB* models, and the last entry belongs to mixed symmetry representations resulting from the crystal-field splitting of the enlarged symmetry group, $SO(3)_{\text{spin-orbit}}\times\mathcal{T}\times U(1)$.

Γ	$\mathcal{Y}_\Gamma$	Point nodes	Line nodes	Cross nodes
E_{1g}	$p_z(p_x+ip_y)$	$\vartheta=0,\pi$	$\vartheta=\frac{\pi}{2}$	
E_{2u}	$p_z(p_x+ip_y)^2$	$\vartheta=0,\pi$	$\vartheta=\frac{\pi}{2}$	
$A_{2u}\oplus B_{1u}$	$A\,p_z\mathrm{Im}\,(p_x+ip_y)^6$		$\varphi_n=n\frac{\pi}{3}$,	$\vartheta=0,\pi\wedge\varphi_n$
	$+iB\,\mathrm{Im}(p_x+ip_y)^3$		$n=0,\ldots,5$	
$A_{1g}\oplus E_{1g}$	$A\,(2p_z^2-p_x^2-p_y^2)$			$\vartheta=\cos^{-1}\frac{\pm 1}{\sqrt{3}}$
	$+i\,E\,p_yp_z$			$\wedge\,\varphi=0,\pi$

pairing in an ''easy-plane,'' i.e., the pairs form triplet states with amplitudes $\Delta_{\Leftarrow}=\Delta_{\Rightarrow}=\Delta(\mathbf{p})$ and $\Delta_{\leftrightarrows}=0$. In the second class, **d** is complex and the spin components of the order parameter spontaneously break time-reversal symmetry. In the general case $\mathbf{\Delta}$ is complex, with $\mathbf{\Delta}\times\mathbf{\Delta}^*\neq 0$, and varies over the Fermi surface. These states are called ''nonunitary'' because the square of the spin-matrix representation of the order parameter is no longer proportional to the unit spin matrix, $[\Delta^\dagger\Delta]_{\alpha\beta}=|\mathbf{\Delta}|^2\,\delta_{\alpha\beta}+i[\mathbf{\Delta}\times\mathbf{\Delta}^*\cdot\boldsymbol{\sigma}]_{\alpha\beta}$. As a consequence the spin degeneracy of the excitation spectrum is lifted and the quasiparticle energy depends on the local pair spin at $\mathbf{p}_f$: $\mathbf{S}_{\rm pair}(\mathbf{p}_f)\sim i\mathbf{\Delta}(\mathbf{p}_f)\times\mathbf{\Delta}(\mathbf{p}_f)^*$.

Whether or not spin-orbit coupling is weak or strong on the energy scale of k_BT_c has important implications for both the orbital and spin components of the order parameter that are allowed by symmetry. Blount[34] and Volovik and Gorkov[33] showed that line nodes are *not required* for odd-parity states when spin-orbit coupling is relevant. However, line nodes in the ab-plane of the Fermi surface are allowed, and required for some representations, if the normal-state spin-orbit interactions lock **d** along the **c** axis of the crystal, i.e., $\mathbf{d}||\mathbf{c}$. Precisely this orientation of **d** was predicted[35] for UPt_3 based on anisotropic paramagnetic limiting.[30] This effect arises from the competition between the condensation energy and the Zeeman energy. For **d** locked along the **c** axis of the lattice the Zeeman energy is pair-breaking for $\mathbf{H}||\mathbf{c}$, giving rise to paramagnetic limiting. However, for $\mathbf{H}\perp\mathbf{c}$ the Zeeman energy, $\mathcal{F}_{\rm Zeeman}\sim(\mathbf{d}\cdot\mathbf{H})^2$, is minimum (vanishes); as a result there is no paramagnetic limit for this field orientation. The anisotropic paramagnetic limiting of H_{c2} is sensitive to the spin structure of the order parameter, but insensitive to the orbital pairing symmetry.[35,36,7,37] The odd-parity E_{2u} representation with strong spin-orbit locking of $\mathbf{d}||\mathbf{c}$ quantitatively accounts for the anisotropy of the paramagnetic limit of H_{c2} observed at low temperatures.

The spin-singlet E_{1g} model appears to be incompatible with both the tetracritical point for $\mathbf{H}\not\perp\mathbf{c}$ and the anisotropic paramagnetic limiting of H_{c2}. However, Park and Joynt[38] argue that there is enough freedom in the E_{1g} model to account for the existing experimental data on H_{c2}. Both E-rep models have recently been challenged by observations of a nearly temperature independent Knight shift for $\mathbf{H}||\mathbf{c}$,[39] which is interpreted in terms of nonunitary, spin-triplet pairing with weak, or no spin-orbit coupling.[40] The authors of Ref. 39 assume that the Knight shift measures the bulk spin susceptibility. If, for simplicity, we ignore the anisotropy of the normal-state susceptibility, then for a given orientation of **d** the spin susceptibility is given by $\chi_{ij}=\chi_N(\delta_{ij}-d_id_j)+\chi_0\,d_id_j$, where χ_N is the normal state spin susceptibility and $\chi_0(T)$ is the spin susceptibility for $\mathbf{H}||\mathbf{d}$, which is suppressed by pair-breaking and vanishes for $T\rightarrow 0$ in the clean limit. For strong spin-orbit coupling with **d** locked along **c** we expect a suppression of the Knight shift for $T<T_c$ for fields $\mathbf{H}||\mathbf{c}$, but no suppression for $\mathbf{H}\perp\mathbf{c}$. However, in the limit of no spin-orbit coupling the Zeeman energy is minimized by *rotation* of **d** perpendicular to the field. This implies that the Knight shift will be temperature independent and given by the normal-state shift for all field orientations. The NMR measurements of the Knight shift[39] appear to be in conflict with anisotropic paramagnetic limiting of H_{c2}. The paramagnetic limit observed for $H_{c2}^{||}$ is a robust, thermodynamic property of bulk single crystals of UPt_3, and a consistent interpretation of the NMR results for the Knight shift data must accommodate anisotropic paramagnetic limiting. This cannot be accomplished with a model of spin-triplet pairing without strong spin-orbit coupling.

Our analysis presented below for the heat capacity and transport measurements is independent of the interpretation of the Knight shift measurements. We show that the heat capacity, low temperature thermal conductivity and transverse sound attenuation data, in addition to the H-T phase diagram, are in quantitative agreement *only* for the odd-parity E_{2u} representation (Table I), independent of the orientation of **d**. In order to demonstrate this fact we present calculations for other models that have been proposed to account for the phase diagram. Thus, in addition to the 2D E-representations we also examine the transport properties of the order parameter models belonging to mixed representations of the D_{6h} point group, i.e., the AB models[18,20] and the AE model.[41] These models were proposed as alternatives to the E-representations to explain the Ginzburg-Landau region of the H-T phase diagram. The most promising candidate of the AB model is the odd parity, spin-triplet model with mixed $A_{2u}\oplus B_{1u}$ symmetry. The orbital order parameter for the A phase has the form, $\Delta_A(\mathbf{p}_f)\sim p_z\,{\rm Im}(p_x+ip_y)^6$, exhibiting an equatorial line node and six longitudinal line nodes. We also analyze the transport properties of the even-parity, spin-singlet $A_{1g}\oplus E_{1g}$ model with an A phase of the form, $\Delta_A(\mathbf{p}_f)\sim(2p_z^2-p_x^2-p_y^2)$, which has a pair of ''tropical'' line nodes located off the equatorial plane. For a more detailed description of the order parameter for these models, see Refs. 41,42.

III. TRANSPORT THEORY

Electronic transport in the superconducting state is sensitive to the nodal structure of the order parameter, $\Delta(\mathbf{p}_f)$. Recent theoretical analyses[43,27,28,42] of low-temperature thermal conductivity data on superconducting UPt_3 (Refs. 10 and 11) have eliminated most of the theoretical models proposed to explain the phase diagram of UPt_3. The nonunitary, spin-triplet pairing states based on a one-dimensional (1D) orbital representation studied so far,[44–47,40] as well as the two-component order parameter models obtained from nearly degenerate one-dimensional representations[20] (''AB models''), are unable to describe, even qualitatively, the temperature dependence and anisotropy of the thermal conductivity at low temperatures. The only pairing models which can account for the thermal conductivity data are the two-dimensional (2D) orbital representations, E_{1g} and E_{2u}, and the $A_{1g}\oplus E_{1g}$ (AE) model. However, the AE model predicts a large ab-plane anisotropy, which has so far not been observed.[42] After it was shown that a nonunitary, spin-triplet state with a 1D orbital basis function was incompatible with the thermal conductivity data,[42] Machida *et al.*[48] modified their weak spin-orbit coupling model by adopting the 2D orbital representation E_{2u}. However, the model of Ref. 48 proposes a spin structure for the order parameter which is in conflict with the observed Pauli limiting of H_{c2} for $\mathbf{H}||\mathbf{c}$, and it predicts a fourth superconducting phase which disagrees with the phase diagram.

Transverse ultrasound is an even more powerful probe of the order parameter and excitation spectrum than the thermal conductivity.[49,12] The attenuation of hydrodynamic sound is determined by the electronic viscosity tensor, which is sensitive to the relative orientation of the polarization, propagation direction and order parameter.[50,51] The broken symmetries of the pairing state give rise to additional anisotropy of the low-energy excitation spectrum that is specific to the pairing state; the selection rules for acoustic absorption reflect these broken symmetries.

In the hydrodynamic limit, $\omega\tau \ll 1$ and $ql \ll 1$, where $l = v_f\tau$ is the quasiparticle mean-free path and τ is the transport collision time, the ultrasonic attenuation is determined by components of the viscosity tensor

$$\alpha(\mathbf{q},\boldsymbol{\varepsilon},T) = (\omega^2/\varrho c_s^3)\ \eta_{ij,kl}(\mathbf{q},\omega)\ \hat{\boldsymbol{\varepsilon}}_i\hat{\mathbf{q}}_j\hat{\boldsymbol{\varepsilon}}_k\hat{\mathbf{q}}_l, \tag{3}$$

where ϱ is the mass density, $c_s = \omega/q$ is the speed of the sound mode with wave vector $\mathbf{q}$ and polarization $\boldsymbol{\varepsilon}$.[52,53] The hydrodynamic limit is achieved even for high-purity single crystals of UPt_3. For the experiments reported in Ref. 12 with propagation $\mathbf{q}||\mathbf{a}$ and polarization $\boldsymbol{\varepsilon}||\mathbf{b}$ the sound frequency is $\omega/2\pi \simeq 165$ MHz, the speed of sound is $c_s \simeq 2.1$ km/s,[30] and the elastic mean free path is $l_{ab} = v_{f,ab}\tau \approx 1.5$ km/s$\times 240$ ps≈ 360 nm,[54] yielding $\omega\tau \approx 0.25$ and $ql_{ab} \approx 0.18$ at $T = 0$. Similarly, for $\mathbf{q}||\mathbf{a}$ and $\boldsymbol{\varepsilon}||\mathbf{c}$ the reported values are $\omega/2\pi \simeq 228$ MHz, $c_s \simeq 1.4$ km/s, and $l_c \approx \sqrt{2.7}l_{ab}$, yielding $\omega\tau \approx 0.34$ and $ql_c \approx 0.61$ at $T = 0$. The parameters ql_c and $\omega\tau$ are a factor of two smaller near T_c than they are at low temperature, since $\tau(T_c) \simeq \tau(0)/2$. Nevertheless, attenuation measurements for $\boldsymbol{\varepsilon}||\mathbf{c}$ are near the borderline of the hydrodynamic regime. Measurements above and below this cross-over regime would be desirable; both for checking the applicability of hydrodynamic results for the attenuation for $\boldsymbol{\varepsilon}||\mathbf{c}$ and for looking for new phenomena in the collisionless regime.

The viscosity and sound attenuation are calculated from the response of the momentum stress tensor to an ionic displacement field $\mathbf{A}(\mathbf{q},\omega) = A(\mathbf{q},\omega)\boldsymbol{\varepsilon}$. For transverse modes $(\mathbf{q}\cdot\boldsymbol{\varepsilon} = 0)$ the stress and viscosity tensors are related in the hydrodynamic limit by[55,56]

$$\Pi_{ij}(\mathbf{q},\omega) = \omega\, q\, A(\mathbf{q},\omega)\ \eta_{ij,kl}(\mathbf{q},\omega)\ \hat{\boldsymbol{\varepsilon}}_k\hat{\mathbf{q}}_l. \tag{4}$$

At low temperatures the transfer of energy and momentum between the ionic lattice and electronic excitations is dominated by the scattering of quasiparticles off impurities or defects. The theory of momentum transport by quasiparticle scattering is formulated in terms of nonequilibrium Green's functions for electronic quasiparticles coupled to the acoustic modes of the lattice. The momentum stress tensor is

$$\Pi_{ij}(\mathbf{q},\omega) = N_f \int \frac{d\epsilon}{8\pi i} \int d\mathbf{p}_f\, [\mathbf{v}_f]_i [\mathbf{p}_f]_j\, \delta g^K(\mathbf{p}_f,\mathbf{q};\epsilon,\omega), \tag{5}$$

where $\mathbf{v}_f$ is the Fermi velocity, $\mathbf{p}_f$ is the Fermi momentum, N_f the density of states at the Fermi surface, and δg^K is the nonequilibrium quasiparticle Green's function, integrated with respect to the quasiparticle energy, $\xi_{\mathbf{p}} \simeq v_f(p - p_f)$; δg^K includes both the changes in the *distribution* of occupied states and the dynamics of the *spectrum* of low-energy excitations (see the Appendix).

IV. TRANSPORT EQUATIONS

We use Keldysh's formulation of the nonequilibrium response theory and calculate the transport properties and related Green's functions in the quasiclassical limit, which is easily achieved in UPt_3 for excitation energies, $(k_BT, \hbar\omega) \ll E_f \approx 1$ meV, and wavelengths long compared to the Fermi wavelength, i.e., $\hbar q \ll p_f$. The central equation for the nonequilibrium Green's function in the quasiclassical limit is a transport equation. For small deviations from equilibrium the transport equation may be linearized in the deviations of the Green's function from its local equilibrium form. Our analysis and notation follows that of Ref. 43, which provides a detailed discussion of the quasiclassical linear response theory, including a complete solution to the *linearized* nonequilibrium transport equations. A summary of these equations, applicable to momentum transport in Fermi-liquid superconductors, is given in the Appendix.

The transport equation for the Green's function includes the acceleration of electronic quasiparticles by the acoustic field and collision terms which transfer momentum between the lattice and the electrons. The stress tensor, and therefore the electronic viscosity which damps the acoustic wave, is calculated from the solution of the transport equation for the nonequilibrium Green's function, δg^K, which is driven by the coupling of quasiparticles to the ionic displacement field, i.e., an externally imposed sound field, $\hat{\sigma}_{\rm ext}(\mathbf{p}_f,\mathbf{q};\omega) = i(\mathbf{v}_f\cdot\mathbf{q})(\mathbf{p}_f\cdot\mathbf{A})\hat{1}$.[55,56] Below we report new results for the electronic shear viscosity for the order parameter models of UPt_3, and new calculations of the anisotropy and temperature dependence of the attenuation which we use to interpret the experimental data for UPt_3.

In the limit of $\omega \to 0$ and for resonant scattering the viscosity tensor simplifies to

$$\eta_{ij,ij} = -\frac{N_f}{8\pi^3 k_B T} \int d\epsilon\, \mathrm{sech}^2(\epsilon/2k_BT) \times \int d\mathbf{p}_f \frac{[\mathbf{v}_f]_i^2 [\mathbf{p}_f]_j^2}{\mathrm{Re}\, C^R} [g_0^R g_0^{R*} - f_0^R f_0^{R*} + \pi^2], \tag{6}$$

where $C^R = -(1/\pi)\sqrt{|\Delta(\mathbf{p}_f)|^2 - (\tilde{\epsilon}^R)^2}$, $g_0^R = \tilde{\epsilon}^R/C^R$, $f_0^R = -\Delta(\mathbf{p}_f)/C^R$, and $\tilde{\epsilon}^R = \epsilon - \frac{1}{4}\,\mathrm{Tr}[\hat{\tau}_3\hat{\sigma}^R_{\rm imp}]$ is the impurity-renormalized energy. In the case of triplet pairing with a unitary order parameter the only change in Eq. (6) is replacement of $\Delta \to \mathbf{\Delta}$ and $f_0^R f_0^{R*} \to \mathbf{f}_0^R \cdot \mathbf{f}_0^{R*}$. See the Appendix for details on the notation.

For a normal metal with a spherical Fermi surface we obtain Pippard's result for the viscosity, $\eta_{ij,ij} = \frac{2}{15} v_f^2 p_f^2 N_f \tau$ for $i \neq j$.[57] Below T_c the sound attenuation drops; for a conventional superconductor, in the limit $ql \ll 1$, the attenuation decreases exponentially for $k_BT \ll \Delta$.[55] But for an unconventional superconductor in which the order parameter vanishes at points or lines on the Fermi surface, the attenuation decreases with temperature as a power law reflecting the spectrum of low-energy excitations near the nodes of the order

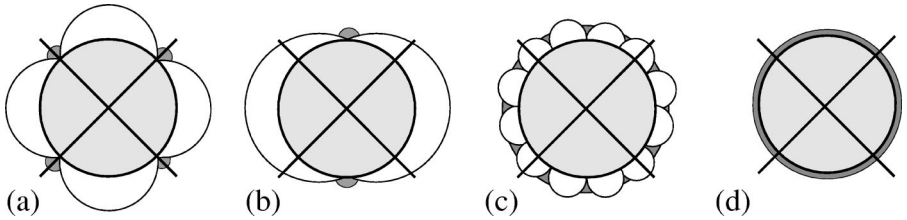

FIG. 2. Sketch of the ϕ dependence of the A phase pairing states at $\vartheta \neq \pi/2$ for (a) E_{2u}, (b) E_{1g}, (c) $A_{2u} \oplus B_{1u}$, and (d) $A_{1g} \oplus E_{1g}$ models. The crossed lines represent the areas of maximal absorption of a sound probe with **ab** symmetry ($\mathbf{q}||\mathbf{a}, \boldsymbol{\varepsilon}||\mathbf{b}$) at the Fermi surface. The dark shaded areas represent the distribution of quasiparticle excitations.

parameter.[50,51,58,59] Impurity scattering modifies this spectrum near the nodes, and at low energies a new energy scale, $\gamma \ll \Delta_0$, appears, which is roughly the ''bandwidth'' of low-energy quasiparticles bound to the impurity distribution by Andreev scattering.[43] The bandwidth also appears as an impurity-renormalized quasiparticle width at zero energy, $\tilde{\epsilon}^R(0) = i\gamma$. This new low energy scale defines a crossover from the power law behavior associated with scattering of continuum quasiparticles for $\gamma/k_B < T \ll T_c$, to a temperature independent attenuation in the limit $k_B T \ll \gamma$.[50,51,58,59]

The bandwidth of the impurity-induced Andreev levels is determined by the self-consistency equation for the quasiparticle self-energy,

$$\gamma = \Gamma_u \frac{\langle \gamma [|\Delta(\mathbf{p}_f)|^2 + \gamma^2]^{-1/2} \rangle}{\cot^2 \delta_0 + \langle \gamma [|\Delta(\mathbf{p}_f)|^2 + \gamma^2]^{-1/2} \rangle^2}, \tag{7}$$

where $\langle \ldots \rangle$ is an average over the Fermi surface and $\Gamma_u = n_{\rm imp}/\pi N_f$ is the scattering rate in the normal state for resonant impurities and δ_0 is the scattering phase shift. For the high purity UPt_3 crystals studied in Ref. 10, i.e., low scattering rate, the crossover temperature is very low compared to T_c; analysis of the thermal conductivity provides a determination of both the scattering phase shift as well as the bandwidth of the impurity-induced Andreev states. The scattering centers are nearly resonant, i.e., $\delta_0 \simeq \pi/2$, giving a bandwidth, and crossover temperature, of order $\gamma \sim k_B T^* \approx 0.2\sqrt{\mu \Gamma_u \Delta_0} \approx 0.07 k_B T_c$, where $\Gamma_u \simeq 0.03 k_B T_c$, $\Delta_0 \simeq 2.0 k_B T_c$ and the slope of the excitation gap near the line node is $\mu = \Delta_0^{-1} |d\Delta/d\vartheta|_{\vartheta=\pi/2} \simeq 2$. Thus, transport experiments on UPt_3 have so far not investigated the ultralow temperature region $k_B T \ll \gamma$ in any systematic way.

V. TRANSVERSE SOUND ATTENUATION

The *anisotropy* and temperature dependence of the sound attenuation is sensitive to the polarization of the sound field and the symmetry of the order parameter. This was the basis of transverse sound attenuation experiments that provided early evidence for a line of nodal excitations in the basal plane.[49] We examine the ab-plane anisotropy of the transverse sound attenuation. Our analysis covers the full temperature range below T_c, and is particularly sensitive to the polarization and anisotropy of the order parameter for both A and B phases of UPt_3. To illustrate the sensitivity of the transverse sound polarization to the order parameter symmetry consider the theoretical models for the A phase of UPt_3. The ab-plane anisotropies of the excitation gap, $|\Delta(\vartheta \neq \pi/2, \phi)|$, for the A phase of four pairing models, E_{2u}, E_{1g}, $A_{2u} \oplus B_{1u}$, and $A_{1g} \oplus E_{1g}$, are shown in Fig. 2.

The propagation and polarization vectors determine the angular dependence of the momentum transport by quasiparticles on the Fermi surface; the matrix element is proportional to $[\mathbf{p}_f]_i^2 [\mathbf{v}_f]_j^2$. This angular dependence is weighted by the angle-resolved density of states for momentum transfer via impurity scattering, which depends on the anisotropy of the quasiparticle excitation spectrum through $|\Delta(\mathbf{p}_f)|^2$. When both the propagation and polarization vectors are in the basal plane ($\mathbf{q}||\mathbf{a}, \boldsymbol{\varepsilon}||\mathbf{b}$)[60] the matrix element is proportional to $\sin^2 2\phi$, and is maximum at angles of $\pi/4$ from these two axes, i.e., the midpoints between the polarization and propagation directions. If these midpoint directions coincide with nodal directions [e.g., $|\Delta(\mathbf{p}_f)| \sim |\cos 2\phi|$ for E_{2u}] then the attenuation will be a maximum, while if the midpoint directions are along the antinodal directions then the attenuation is a minimum. This is illustrated in Fig. 2 where the polarization is directed along the **a** direction. The attenuation is largest when the *polarization* is along an antinode of the order parameter, and it is smallest when the polarization is along a nodal direction. One can immediately see that we should expect to observe a rather different ab-plane angular dependence to the attenuation for the different order parameter models proposed for UPt_3. We quantify these remarks below.

A. Results

In order to make quantitative predictions for UPt_3 we use heat capacity and thermal conductivity measurements to fix the magnitude of the order parameter, the Fermi surface anisotropy, the nodal parameters and the scattering rate, all of which control the temperature dependence and anisotropy of the thermal conductivity below T_c.[27,42] We used variational basis functions based on the polynomial functions in Table I. Symmetry dictates the geometry of the line and point nodes, as well as the topological indices for the point nodes, but not the slopes or curvature of the nodal regions of the excitation gap. Our variational procedure fits these parameters to the low-energy excitation spectrum from the thermal conductivity data of Ref. 10. The order parameter is then determined self-consistently. For a detailed discussion of this analysis see Refs. 27 and 42. The anisotropy and temperature dependence of the transverse sound attenuation are then calculated with no additional parameters or adjustments of the order parameter models shown in Fig. 2.

The transition temperature and splitting of the zero-field transition in UPt_3 determine the scale and relative magnitudes of the two order parameter components; they determine the dominant and subdominant instability temperatures.

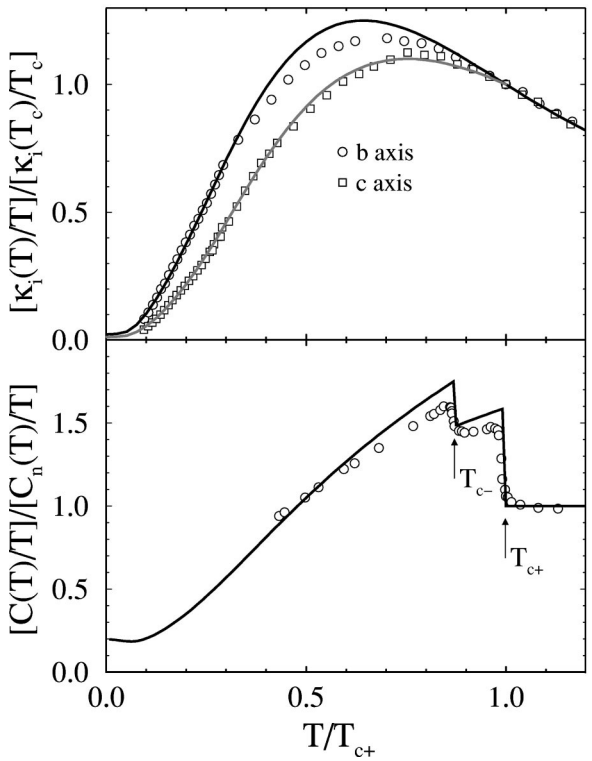

FIG. 3. Fit of the E_{2u} model to the thermal conductivity data (top) (Ref. 10) and the specific heat data (bottom) (Ref. 9).

The instability temperature for the dominant channel is the transition temperature, $T_{c1}=T_{c+}$, while the second instability temperature represents the strength of the subdominant pairing channel, $T_{c2}\propto\omega_c\exp(-1/V_2)$, where V_2 is the pairing interaction for the sub-dominant channel and ω_c is the cutoff energy.[61] The physical transition temperature, T_{c-}, separating the A and B phases depends on the relative strength of the two paring channels, i.e., on $T_{c2}/T_{c+}\leqslant 1$. We solve the coupled gap equations for the first and second transition and adjust T_{c2} to the observed splitting in the specific heat, $(T_{c+}-T_{c-})/T_{c+}\approx 60\,\mathrm{mK}/495\,\mathrm{mK}$.[12,9] All other material parameters are taken from our previous analysis of the thermal conductivity of UPt_3.[42] We show the quality of the theoretical fits to the thermal conductivity, κ, and heat capacity for the E_{2u} model in Fig. 3. Similar fits can be obtained for the E_{1g} and AE models. However, only the in-plane thermal conductivity data can be accounted for by the AB model.

1. Identification of the A phase

In Fig. 4 we show the attenuation data reported by Ellman *et al.*[12] for transverse sound propagation in the ab plane with $\mathbf{q}||\mathbf{a}$ and polarizations both in and out of plane, $\boldsymbol{\varepsilon}||\mathbf{b}$ and $\boldsymbol{\varepsilon}||\mathbf{c}$. These measurements were made on the same batch of crystals of UPt_3 as the heat capacity and thermal conductivity measurements shown in Fig. 2. In addition to the anisotropy associated with the polarization, the data show a pronounced change in the anisotropy and temperature dependence at the A-B phase transition.

The enhanced absorption in the A phase compared to that of the B phase at the same temperature results from excess quasiparticles that scatter off the impurity distribution due to

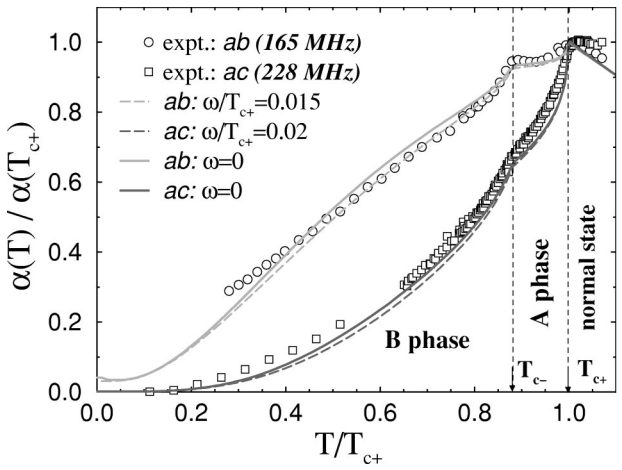

FIG. 4. Comparison between the measured and calculated transverse sound attenuation of UPt_3. The theoretical calculation is for the E_{2u} model and the phenomenological model previously used for the total elastic and inelastic scattering rate, $\Gamma(T)=0.03k_BT_{c+}(1+T^2/T_{c+}^2)$, obtained from the thermal conductivity analysis. The data are from Ellman *et al.* (Ref. 12) which are corrected to vanish at $T=0$.

additional nodes of the A phase order parameter compared to that of the B phase. Below T_{c-} the subdominant order parameter closes the additional nodes of the A phase order parameter. Thus, the sound absorption drops faster in the B phase than it would in the A phase. The experimental results for the sound attenuation, including the anomaly at T_{c-}, are in excellent agreement with theoretical calculations for the E_{2u} model of the A and B phases, with an A phase given by a $\boldsymbol{\eta}=(1,0)$ state, but not a $(0,1)$ state; and a B phase at low temperature which is (approximately) the $\boldsymbol{\eta}=(1,\pm i)$ state.[62] The comparison between theory and experiment is unsatisfactory for all other models. Even including the frequency dependence of the viscosity, $\eta_{ij,ij}(\mathbf{q},\omega)$, does not change this result. We find only minor corrections to the sound attenuation for $\omega\ll\Delta_0$ (see Fig. 4). The $(1,0)$ state of the A phase, as determined by sound attenuation, also agrees with the order parameter orientation obtained from the observed sixfold oscillations of $H_{c2}(\phi)$, and the change in sign of these oscillations when crossing the A-C phase boundary.[63]

In Fig. 5 we show the sound attenuation for **ab** and **ac** polarizations and different pairing models. Note in particular that none of the order parameter models shown in Fig. 5 can account for both anomalies in $\alpha_{\mathbf{ab}}$ and $\alpha_{\mathbf{ac}}$ at T_{c-}. The main result of this work is that the experimental data for the heat capacity, thermal conductivity, and sound attenuation, as well as the H-T phase diagram, are explained *only* by an order parameter with an orbital E_{2u} pairing symmetry. We emphasize that there are no adjustable parameters in the calculation of the sound attenuation; all parameters of the model were previously determined by fitting the theoretical model parameters to the heat capacity and thermal conductivity.[42]

2. Domain structure

Neutron diffraction studies in pure UPt_3 under pressure,[22] and at ambient pressure in Pd doped samples $(Pt\leftrightarrow Pd)$,[64] demonstrated that the splitting of T_c correlates with the basal plane AFM, suggesting a SBF coupling between the super-

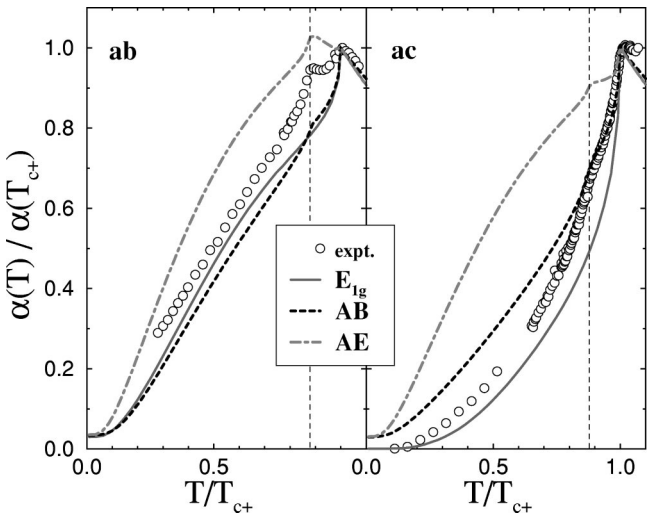

FIG. 5. Attenuation of **ab** and **ac** transverse sound for the various order parameter models.

conducting and AFM order. It has been argued, based on neutron diffraction studies as a function of magnetic field, that the AFM order is described either by a distribution of three equally populated domains, with **Q** vectors oriented 120° to one another, or a triple-**Q** structure.[65,66] If a domain structure is present then, in the AFM model for the SBF, the superconducting order parameter describing the *A* phase in the *E*-rep models may also form a domain structure. Such a domain structure leads to a weakening of the anomaly for $\alpha_{\mathbf{ab}}$ at T_{c-}, but leaves the anomaly in $\alpha_{\mathbf{ac}}(T_{c-})$ virtually unchanged.

In Fig. 6 we show the effect of multidomain averaging on the anisotropy of the transverse sound attenuation. These calculations show that an AFM domain structure does not destroy the anomaly in the attenuation at T_{c-}. However, averaging over domains suppresses the characteristic enhancement of $\alpha_{\mathbf{ab}}$ for the E_{2u} order parameter coupled to a dominant or single domain of the SBF. In particular, the domain-averaged attenuation, $\langle \alpha_{\mathbf{ab}} \rangle$, for the E_{2u} pairing state drops roughly twice as fast as the measured attenuation in the *A* phase. If the AFM order parameter is the SBF for the superconducting phases, then our calculations are in agreement with transport and heat capacity measurements only for an E_{2u} order parameter coupled to a *dominant* domain, or a triple-**Q** structure for the antiferromagnetic SBF.[26]

3. Scattering phase shifts

It has been pointed out in several studies that the temperature dependence of the transport coefficients in UPt_3 is qualitatively consistent with strong scattering in the unitarity limit. Our analysis of the thermal conductivity data,[10] and the attenuation data[12] confirm that the scattering phase shift is near the resonant limit; from the analysis of the thermal conductivity we obtain $\delta_0 \geqslant 80°$,[27] while the transverse sound attenuation data implies a scattering phase shift $\delta_0 > 60°$, as shown in Fig. 7.

4. Ultralow temperature region

The temperature dependence of the transverse sound attenuation is predicted to change qualitatively below the

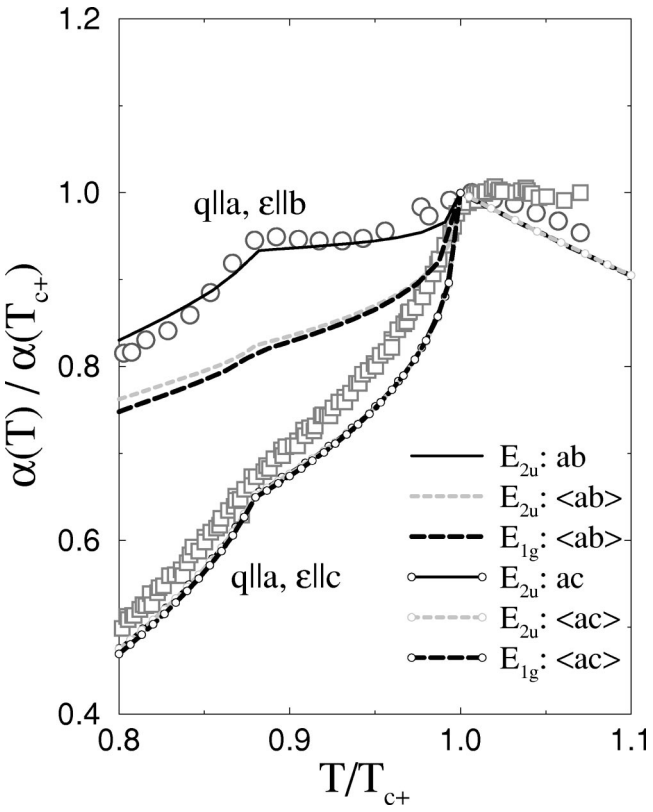

FIG. 6. Configuration averaged attenuation (indicated by $\langle \ldots \rangle$) assuming three equally populated monodomains for an E_{1g} and E_{2u} pairing state. For a comparison the results for the E_{2u} state of Fig. 4 are replotted.

cross-over temperature, $k_B T < \gamma$. The zero-temperature limit is finite, reflecting the finite density of states at the Fermi level, and the leading temperature-dependent corrections are of the Sommerfeld type, $\mathcal{O}[(T/\gamma)^2]$ for $k_B T < \gamma$. The limiting attenuation in the ultralow temperature limit, $k_B T \ll \gamma$, is obtained from the viscous stress tensor for $T \to 0$ and $\omega \to 0$. In this limit the states contributing to the stress tensor in Eq. (5) are confined to the impurity-induced Andreev band of order $\gamma \gg \max(T, \omega)$. The spectrum and self-energy are

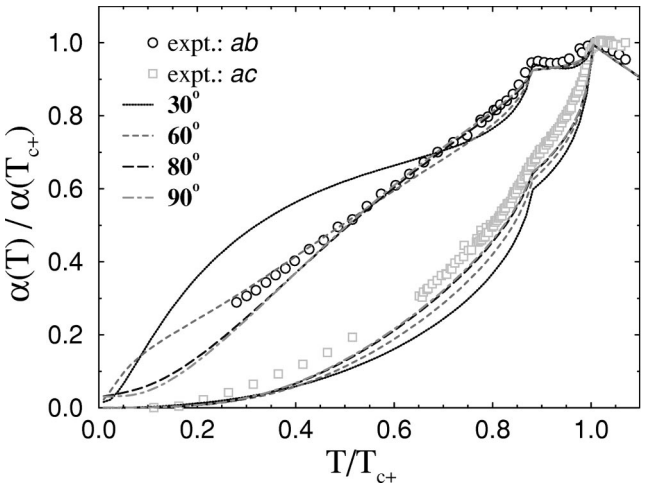

FIG. 7. Sensitivity of the transverse sound attenuation to the scattering phase shift $\delta_0 = 30°, 60°, 80°, 90°$ for the E_{2u} pairing model and the same parameters as shown in Fig. 4.

TABLE II. Asymptotic low-temperature limits of the sound attenuation ($\omega,\ T\to 0$) and thermal conductivity for the E_{1g} and E_{2u} pairing states. The results are scaled in units of $\kappa_0=(\pi^2/3)k_B^2 T N_f v_f^2 \tau_\Delta$ and $\alpha_0=(\omega^2/4\varrho\, c_s^3)p_f^2 N_f v_f^2 \tau_\Delta$, where $\tau_\Delta \equiv \hbar/2\mu\Delta_0$ is an effective transport time.

Transport coefficient	E_{1g}	E_{2u}
$\kappa_{\mathbf{bb}}/\kappa_0$	1	1
$\kappa_{\mathbf{cc}}/\kappa_0$	$2\mu\gamma/(\mu_1^2\Delta_0)$	μ/μ_2
$\alpha_{\mathbf{ab}}/\alpha_0$	1	1
$\alpha_{\mathbf{ac}}/\alpha_0$	$\dfrac{8\mu}{1+2\mu^2}\dfrac{\Gamma_u}{\Delta_0}$ [a]	$\dfrac{2\mu}{\mu_2^2}\dfrac{\gamma}{\Delta_0}$

[a]In the strong scattering limit including vertex corrections.

weakly energy dependent on this scale, thus, we can evaluate the slowly varying parts of the integrand in Eq. (6) at zero energy to obtain

$$\eta_{ij,ij}\simeq N_f\int d\mathbf{p}_f\,[\mathbf{v}_f]_i^2[\mathbf{p}_f]_j^2\frac{\gamma^2}{[|\Delta(\mathbf{p}_f)|^2+\gamma^2]^{3/2}}, \qquad (8)$$

where we have neglected the Sommerfeld corrections of order $\mathcal{O}[(T/\gamma)^2]$.[67]

Whether or not the zero-temperature limit is *universal*, i.e., independent of the density and scattering cross section for the impurities, depends on the polarization of the acoustic wave and the symmetry of the ground state. The damping is universal only for transverse waves propagating along the high symmetry directions in the ab plane, i.e., for polarization $\boldsymbol{\varepsilon}||\mathbf{b}$ propagating along $\mathbf{q}||\mathbf{a}$, or vice versa. For these polarizations the ground state of *all* the models we discuss, except the AE model, possess a *universal* limit for the attenuation. Table II summarizes the results for the E_{1g} and E_{2u} models. For the ground state of either E-representation we find $\eta_{\mathbf{ab},\mathbf{ab}}\simeq v_f^2 p_f^2 N_f/(8\mu\Delta_0)$, where $\mu\approx 2$ is the slope of the excitation gap near the line node in the ab plane. For any other polarization the relevant viscosity is nonuniversal for $\omega, T\ll\gamma$. For example, for the E_{2u} ground state we obtain a limiting value for $\alpha_{\mathbf{ac}}(0)\approx(2\mu\gamma/\mu_2^2\Delta_0)\alpha_{\mathbf{ab}}(0)\ll\alpha_{\mathbf{ab}}(T_{c+})$, where $\mu_2\approx 4$ is the parameter defining the curvature of the excitation gap near the quadratic point node along the **c** axis.[68]

Further experiments using transverse sound can be used to confirm the predictions for the ab-plane anisotropy of the order parameter in UPt_3. The ideal method would be to propagate transverse sound along the **c** axis and measure the attenuation as a function of the azimuthal orientation of the polarization in the ab plane. The qualitative predictions for the in-plane anisotropy can be deduced from Fig. 2; a twofold symmetry of the anomaly at T_{c-} is expected for the E_{1g} representation and a nearly isotropic attenuation above T_{c-} for the other models. In the B phase all models show a nearly isotropic attenuation except for the AE model, which has a twofold symmetry. A similar experiment was suggested by Moreno and Coleman[69] to map out the gap structure in the high-T_c cuprates.

To summarize the main conclusions, we have shown that transverse ultrasound provides detailed information on the orbital pairing symmetry of both the superconducting A and B phases of UPt_3; the anisotropy and the anomalies in the temperature dependence of the attenuation for different polarizations is explained *only* by an E_{2u} order parameter. Measurements of $\alpha_{\mathbf{ab}}$ and $\alpha_{\mathbf{ac}}$ are in excellent agreement with a (1,0) state for the A phase, corresponding to a $p_z(p_x^2-p_y^2)$ order parameter. Further measurements at lower temperatures, or as a function of impurity disorder, may also be used to test the prediction of a universal limit for the in-plane transverse sound attenuation.

ACKNOWLEDGMENTS

This research was supported by NSF Grants No. DMR 9705473 and No. DMR 91-20000 through the Science and Technology Center for Superconductivity. M.J.G. also acknowledges support from the Los Alamos National Laboratory under the auspices of the Department of Energy. We also thank the Aspen Center for Physics where part of this research was carried out.

APPENDIX

In this appendix we summarize the relevant nonequilibrium transport equations for our calculations of the sound attenuation in unconventional superconductors. For a more extensive review of nonequilibrium transport theory in superconductors see Refs. 43 and 70.

The nonequilibrium (Keldysh) Green's function,

$$\delta\hat{g}^K=\delta\hat{g}^R\circ\Phi_0-\Phi_0\circ\delta\hat{g}^A+\delta\hat{g}^a, \qquad (A1)$$

contains the *spectral response* given by the retarded and advanced Green's functions ($\delta\hat{g}^{R,A}$), and the *anomalous response* given by $\delta\hat{g}^a$, which in normal metals is essentially the nonequilibrium distribution function. The equilibrium distribution function is $\Phi_0=\tanh(\epsilon/2k_BT)$, and we use the shorthand notation for the shifting product, $\Phi_0\circ A=\Phi_0(\epsilon-\omega/2)A(\epsilon,\omega)$ and $A\circ\Phi_0=A(\epsilon,\omega)\Phi_0(\epsilon+\omega/2)$. Pairing correlations and particle-hole coherence require a matrix structure for the particle-hole degree of freedom. The ''hat'' over the Green's functions and self-energies indicates their 4×4 matrix structure in particle-hole and spin space.

The transport equations for the Green's functions, linearized with respect to an external perturbation, are

$$[\delta\hat{g}^{R,A},\hat{h}^{R,A}]_\circ=[\hat{g}_0^{R,A},\hat{\sigma}_{\rm ext}+\delta\hat{\sigma}^{R,A}]_\circ, \qquad (A2)$$

$$\begin{aligned}\hat{h}^R\circ\delta\hat{g}^a-\delta\hat{g}^a\circ\hat{h}^A&=\delta\hat{\sigma}^a\circ\hat{g}_0^A-\hat{g}_0^R\circ\delta\hat{\sigma}^a\\&\quad-[\hat{\sigma}_{\rm ext},\Phi_0]_\circ\circ\hat{g}_0^A-\hat{g}_0^R\circ[\Phi_0,\hat{\sigma}_{\rm ext}]_\circ, \qquad (A3)\end{aligned}$$

where $\hat{h}^{R,A}=\epsilon\hat{\tau}_3-\hat{\sigma}_0^{R,A}$, $\hat{\tau}_3$ is a Pauli matrix, and $\hat{\sigma}_{\rm ext}$ is the external perturbation, e.g., the coupling of quasiparticles to a sound field (ionic displacement field). The transport equations determine the deviations of the Green's functions from

their local equilibrium values, $\delta\hat{g}^X=\hat{g}^X-\hat{g}_0^X$, in terms of the external field and the corrections to the self-energies, $\delta\hat{\sigma}^X=\hat{\sigma}^X-\hat{\sigma}_0^X$ with $X\in\{R,A,K\}$. The anomalous self-energy, $\delta\hat{\sigma}^a$, is defined similarly to the $\delta\hat{g}^a$,

$$\delta\hat{\sigma}^K=\delta\hat{\sigma}^R\circ\Phi_0-\Phi_0\circ\delta\hat{\sigma}^A+\delta\hat{\sigma}^a. \tag{A4}$$

The equilibrium Green's functions, $\hat{g}_0^X$, and self-energies, $\hat{\sigma}_0^X$, are inputs to the linearized transport equations. At low temperatures, and for long-wavelength, low-frequency sound, the damping of the acoustic wave is determined by the scattering of quasiparticles off impurities and defects that are comoving with the ionic lattice.[55] Impurity scattering enters the transport equations via the impurity-scattering self-energies,

$$\hat{\sigma}^X(\mathbf{p}_f;\epsilon,t)=n_{\rm imp}\hat{t}^X(\mathbf{p}_f,\mathbf{p}_f;\epsilon,t), \tag{A5}$$

where the quasiparticle-impurity scattering t-matrices are given by

$$\hat{t}^{R,A}(\mathbf{p}_f,\mathbf{p}_f';\epsilon,t)=\hat{u}(\mathbf{p}_f,\mathbf{p}_f')+N_f\langle\hat{u}(\mathbf{p}_f,\mathbf{p}_f'')\circ\hat{g}^{R,A}(\mathbf{p}_f'';\epsilon,t)\circ\hat{t}^{R,A}(\mathbf{p}_f'',\mathbf{p}_f';\epsilon,t)\rangle_{\mathbf{p}_f''}, \tag{A6}$$

$$\hat{t}^K(\mathbf{p}_f,\mathbf{p}_f';\epsilon,t)=N_f\langle\hat{t}^R(\mathbf{p}_f,\mathbf{p}_f'';\epsilon,t)\circ\hat{g}^K(\mathbf{p}_f'';\epsilon,t)\circ\hat{t}^A(\mathbf{p}_f'',\mathbf{p}_f';\epsilon,t)\rangle_{\mathbf{p}_f''}. \tag{A7}$$

The t-matrices are calculated self-consistently with the order parameter, $\hat{\Delta}(\mathbf{p}_f)$, and with the impurity vertex, $\hat{u}(\mathbf{p}_f,\mathbf{p}_f')$, describing elastic coupling of quasiparticles to impurities. The calculations presented here assume isotropic, nonmagnetic impurities with $\hat{u}=u_0\hat{1}$ for all $(\mathbf{p}_f,\mathbf{p}_f')$. This model is then described by two parameters, e.g., the s-wave scattering phase shift, $\delta_0=\tan^{-1}(\pi N_f u_0)$, and the density of impurities, $n_{\rm imp}$. Another useful parametrization is in terms of the cross section, $\sigma=(4\pi/k_f^2)\sin^2\delta_0$, and the normal-state scattering rate in the unitarity limit ($\delta_0=\pi/2$), $\Gamma_u=n_{\rm imp}/\pi N_f$. Note that the transport scattering rate in this model is given by $1/2\tau=\Gamma_u\sin^2\delta_0$, and the elastic mean free path is then $l_{\rm el}=v_f\tau$.

The other key term entering the transport equations is the off-diagonal pairing self-energy, or order parameter. The general form for the pairing self-energies is

$$\hat{\Delta}^{R,A}=\begin{pmatrix}0 & \Delta i\sigma_y+\mathbf{\Delta}\cdot i\boldsymbol{\sigma}\sigma_y\\ \overline{\Delta} i\sigma_y+\overline{\mathbf{\Delta}}\cdot i\sigma_y\boldsymbol{\sigma} & 0\end{pmatrix}, \tag{A8}$$

where the spin-singlet (Δ) and spin-triplet ($\mathbf{\Delta}$) order parameters are given by the gap equations,

$$\Delta^{R,A}(\mathbf{p}_f;t)=\int\frac{d\epsilon}{4\pi i}\langle V^s(\mathbf{p}_f,\mathbf{p}_f')\,f^K(\mathbf{p}_f';\epsilon,t)\rangle_{\mathbf{p}_f'}, \tag{A9}$$

$$\mathbf{\Delta}^{R,A}(\mathbf{p}_f;t)=\int\frac{d\epsilon}{4\pi i}\langle\underline{\mathbf{V}}^t(\mathbf{p}_f,\mathbf{p}_f')\cdot\mathbf{f}^K(\mathbf{p}_f';t)\rangle_{\mathbf{p}_f'}, \tag{A10}$$

where V^s and $\mathbf{V}^t$ are the pairing interactions in the singlet and triplet channels. The components $\overline{\Delta}$ and $\overline{\mathbf{\Delta}}$ are related to Δ and $\mathbf{\Delta}$ by fundamental symmetries (see Appendix C of Ref. 71); in equilibrium $\overline{\Delta}=\Delta^*$ and $\overline{\mathbf{\Delta}}=\mathbf{\Delta}^*$.

To complete the set of equations for the linear response equations we write the solutions for the equilibrium response functions in terms of renormalized quasiparticle energy and order parameter. For spin-singlet and unitary spin-triplet pairing the general solutions for the equilibrium retarded and advanced Green's functions are

$$\hat{g}_0^{R,A}=-\pi\frac{\tilde{\epsilon}^{R,A}\hat{\tau}_3-\hat{\tilde{\Delta}}^{R,A}}{\sqrt{|\tilde{\Delta}^{R,A}|^2-(\tilde{\epsilon}^{R,A})^2}}, \tag{A11}$$

where the renormalized quasiparticle energy is

$$\tilde{\epsilon}^{R,A}(\mathbf{p}_f,\epsilon)=\epsilon-\tfrac{1}{4}\,\mathrm{Tr}[\hat{\tau}_3\hat{\sigma}_{\rm imp}^{R,A}(\mathbf{p}_f,\epsilon)]. \tag{A12}$$

For resonant s-wave scattering

$$\hat{\sigma}_{\rm imp}^{R,A}(\epsilon)=-\Gamma_u\langle\hat{g}_0^{R,A}(\mathbf{p}_f;\epsilon)\rangle_{\mathbf{p}_f}^{-1}. \tag{A13}$$

For s-wave scattering the renormalization of the off-diagonal self-energy by impurity scattering vanishes,

$$\hat{\tilde{\Delta}}^{R,A}(\mathbf{p}_f,\epsilon)=\hat{\Delta}(\mathbf{p}_f), \tag{A14}$$

for nonidentity representations of the point group, i.e., excluding the A_{1g} representation. Finally, we note that the diagonal component of the nonequilibrium Green's function that determines the momentum stress tensor in Eq. (5) is obtained from the matrix Green's function by $\delta g^K=\frac{1}{4}\,\mathrm{Tr}\,\delta\hat{g}^K$.

[1] H. Ott, H. Rudigier, Z. Fisk, and J. Smith, Phys. Rev. Lett. **50**, 1595 (1983).

[2] G. Stewart, Z. Fisk, J. Willis, and J. Smith, Phys. Rev. Lett. **52**, 679 (1984).

[3] V. Müller, Ch. Roth, E. W. Scheidt, K. Lüders, E. Bucher, and H. E. Bömmel, Phys. Rev. Lett. **58**, 1224 (1987).

[4] Y. J. Qian, M. F. Xu, A. Schenstrom, H. P. Baum, J. B. Ketterson, D. Hinks, M. Levy, and B. K. Sarma, Solid State Commun. **63**, 599 (1987).

[5] R. A. Fisher, S. Kim, B. F. Woodfield, N. E. Phillips, L. Taillefer, K. Hasselbach, J. Flouquet, A. L. Giorgi, and J. L. Smith, Phys. Rev. Lett. **62**, 1411 (1989).

[6] R. Hasselbach, L. Taillefer, and J. Flouquet, Phys. Rev. Lett. **63**, 93 (1989).

[7] J. A. Sauls, Adv. Phys. **43**, 113 (1994).

[8] R. Heffner and M. R. Norman, Comments Condens. Matter Phys. **17**, 361 (1996).

[9] L. Taillefer, B. Ellman, B. Lussier, and M. Poirier, Physica B **230**, 327 (1997); includes the specific heat data by M. Sieck and H. von Löhneysen.

[10] B. Lussier, B. Ellman, and L. Taillefer, Phys. Rev. B **53**, 5145 (1996).
[11] H. Suderow, J. P. Brison, A. Huxley, and J. Flouquet, J. Low Temp. Phys. **108**, 11 (1997).
[12] B. Ellman, L. Taillefer, and M. Poirier, Phys. Rev. B **54**, 9043 (1996).
[13] G. Bruls, D. Weber, P. Thalmeier, and B. Lüthi, Phys. Rev. Lett. **65**, 2294 (1990).
[14] S. Adenwalla, S. W. Lin, Q. Z. Ran, Z. Zhao, J. B. Ketterson, J. A. Sauls, L. Taillefer, D. G. Hinks, M. Levy, and B. K. Sarma, Phys. Rev. Lett. **65**, 2298 (1990).
[15] D. W. Hess, T. Tokuyasu, and J. A. Sauls, J. Phys.: Condens. Matter **1**, 8135 (1989).
[16] K. Machida and M. Ozaki, J. Phys. Soc. Jpn. **58**, 2244 (1989).
[17] S. K. Sudaram and R. Joynt, Phys. Rev. B **40**, 8780 (1989).
[18] I. Luk'yanchuk, J. Phys. I **1**, 1155 (1991).
[19] M. R. Norman, Physica C **194**, 203 (1992).
[20] D. Chen and A. Garg, Phys. Rev. Lett. **70**, 1689 (1993).
[21] R. Heid, Y. B. Bazaliy, V. Martisovits, and D. L. Cox, Phys. Rev. Lett. **74**, 2571 (1995).
[22] S. M. Hayden, L. Taillefer, C. Vettier, and J. Flouquet, Phys. Rev. B **46**, 8675 (1992).
[23] P. A. Midgley, S. M. Hayden, L. Taillefer, B. Bogenberger, and H. von Löhneysen, Phys. Rev. Lett. **70**, 678 (1993).
[24] V. P. Mineev, Pis'ma Zh. Éksp. Theor. Fiz. **57**, 659 (1993) [JETP Lett. **57**, 680 (1993)].
[25] B. Ellman, M. Sutton, B. Lussier, R. Bruning, L. Taillefer, and S. Hayden, cond-mat/9704125 (unpublished).
[26] Existing neutron scattering data on UPt_3 is inconclusive on the precise structure of the AFM phase. Triple-**Q** and multidomain structures are discussed in a recent e-print by J. Moreno and J. A. Sauls, cond-mat/0004253 (unpublished).
[27] M. J. Graf, S.-K. Yip, and J. A. Sauls, J. Low Temp. Phys. **102**, 367 (1996); **106**, 727(E) (1997).
[28] M. R. Norman and P. J. Hirschfeld, Phys. Rev. B **53**, 5706 (1996).
[29] A. Fledderjohann and P. J. Hirschfeld, Solid State Commun. **94**, 163 (1995).
[30] B. Shivaram, T. Rosenbaum, and D. Hinks, Phys. Rev. Lett. **57**, 1259 (1986).
[31] N. Keller, J. L. Tholence, A. Huxley, and J. Flouquet, Phys. Rev. Lett. **73**, 2364 (1994).
[32] P. W. Anderson, Phys. Rev. B **30**, 4000 (1984).
[33] G. E. Volovik and L. P. Gor'kov, Sov. Phys. JETP **61**, 843 (1985) [Zh. Éksp. Teor. Fiz. **88**, 1412 (1985)].
[34] E. Blount, Phys. Rev. B **32**, 2935 (1985).
[35] C. H. Choi and J. A. Sauls, Phys. Rev. Lett. **66**, 484 (1991).
[36] C. H. Choi and J. A. Sauls, Phys. Rev. B **48**, 13 684 (1993).
[37] G. Yang and K. Maki, Europhys. Lett. **48**, 206 (1999).
[38] K. Park and R. Joynt, Phys. Rev. B **53**, 12 346 (1996).
[39] H. Tou, Y. Kitaoka, K. Ishida, K. Asayama, N. Kimura, Y. Onuki, E. Yamamoto, Y. Haga, and K. Maezawa, Phys. Rev. Lett. **80**, 3129 (1998).
[40] K. Machida and T. Ohmi, J. Phys. Soc. Jpn. **67**, 1122 (1998).
[41] M. Zhitomirskii and K. Ueda, Phys. Rev. B **53**, 6591 (1996).
[42] M. J. Graf, S.-K. Yip, and J. A. Sauls, J. Low Temp. Phys. **114**, 257 (1999).
[43] M. J. Graf, S.-K. Yip, J. A. Sauls, and D. Rainer, Phys. Rev. B **53**, 15 147 (1996).
[44] K. Machida and M. Ozaki, Phys. Rev. Lett. **66**, 3293 (1991).
[45] T. Ohmi and K. Machida, Phys. Rev. Lett. **71**, 625 (1993).
[46] K. Machida, T. Ohmi, and M. Ozaki, J. Phys. Soc. Jpn. **62**, 3216 (1993).
[47] K. Machida and T. Ohmi, J. Phys. Soc. Jpn. **65**, 3456 (1996).
[48] K. Machida, T. Nishira, and T. Ohmi, J. Phys. Soc. Jpn. **68**, 3364 (1999).
[49] B. Shivaram, Y. Jeong, T. Rosenbaum, and D. Hinks, Phys. Rev. Lett. **56**, 1078 (1986).
[50] S. Schmitt-Rink, K. Miyake, and C. Varma, Phys. Rev. Lett. **57**, 2575 (1986).
[51] P. J. Hirschfeld, D. Vollhardt, and P. Wölfle, Solid State Commun. **59**, 111 (1986).
[52] W. P. Mason, Phys. Rev. **97**, 557 (1955).
[53] L. D. Landau and I. M. Lifshitz, *Fluid Mechanics*, 1st ed., Course in Theoretical Physics (Pergamon, New York, 1959), Vol. 6.
[54] J. B. Kycia, J. I. Hong, M. J. Graf, J. A. Sauls, D. N. Seidman, and W. P. Halperin, Phys. Rev. B **58**, R603 (1998).
[55] T. Tsuneto, Phys. Rev. **121**, 402 (1960).
[56] L. Kadanoff and I. Falko, Phys. Rev. **136**, A1170 (1964).
[57] A. B. Pippard, Philos. Mag. **46**, 1104 (1955).
[58] C. J. Pethick and D. Pines, Phys. Rev. Lett. **57**, 118 (1986).
[59] H. Monien, K. Scharnberg, L. Tewordt, and D. Walker, Solid State Commun. **61**, 581 (1987).
[60] We follow the notation for the crystallographic directions used in experiments: $\mathbf{a}||\hat{x}$ and $\mathbf{b}||\hat{y}$.
[61] In the 2D E-rep models the splitting of T_c is related to a weak symmetry breaking field, either due to the antiferromagnetic order or structural modulations or uniaxial stress.
[62] A short report of these results was presented by M. J. Graf, S.-K. Yip, and J. A. Sauls, *International Conference on Low Temperature Physics, Helsinki, August 1999* [Physica B **280**, 176 (2000)].
[63] J. A. Sauls, Phys. Rev. B **53**, 8543 (1996).
[64] R. J. Keizer, A. de Visser, M. J. Graf, A. A. Menovsky, and J. J. Franse, Phys. Rev. B **60**, 10 527 (1999).
[65] B. Lussier, L. Taillefer, W. J. L. Buyers, T. E. Mason, and T. Petersen, Phys. Rev. B **54**, R6873 (1996).
[66] N. H. van Dijk, B. Fåk, L. P. Regnault, A. Huxley, and M. T. Fernandez Diaz, Phys. Rev. B **58**, 3186 (1998).
[67] M. J. Graf, S.-K. Yip, and J. A. Sauls, Czech. J. Phys. **46**, 1005 (1996). For isotropic scattering impurity vertex corrections vanish for most of the ground state order parameters we consider. The *AE* model and the *B* phase of an E_{1g} model are exceptions. The vertex correction for the E_{1g} model is of order $\Delta\eta_{\mathbf{ac},\mathbf{ac}}(0) \sim -2\Gamma_u/(\Delta_0\mu_{\rm line}^3)\ \eta_{\mathbf{ab},\mathbf{ab}}(0)$, which is typically very small and is neglected here.
[68] These asymptotic limits also imply that care must be taken when analyzing the low-T sound attenuation. In particular a more sophisticated procedure for subtracting the background attenuation is required than for conventional BCS superconductors, where it is sufficient to demand that α vanishes as $T\rightarrow 0$.
[69] J. Moreno and P. Coleman, Phys. Rev. B **53**, R2995 (1996).
[70] D. Rainer and J. A. Sauls, in *Superconductivity: From Basic Physics to New Developments*, edited by P. N. Butcher and Y. Lu (World Scientific, Singapore, 1995), pp. 45–78.
[71] J. W. Serene and D. Rainer, Phys. Rep. **101**, 221 (1983).